Neuron
Article

Attentional Stimulus Selection through Selective Synchronization between Monkey Visual Areas

Conrado A. Bosman,[1,2,7,*] Jan-Mathijs Schoffelen,[1,7] Nicolas Brunet,[1] Robert Oostenveld,[1] Andre M. Bastos,[1,3,4] Thilo Womelsdorf,[1] Birthe Rubehn,[5] Thomas Stieglitz,[5] Peter De Weerd,[1,6] and Pascal Fries[1,3,*]
[1]Donders Institute for Brain, Cognition, and Behaviour, Radboud University Nijmegen, 6525 EN Nijmegen, Netherlands
[2]Cognitive and System Neuroscience Group, Swammerdam Institute for Life Sciences, Center for Neuroscience, University of Amsterdam, 1098 XH Amsterdam, Netherlands
[3]Ernst Strüngmann Institute (ESI) for Neuroscience in Cooperation with Max Planck Society, 60528 Frankfurt, Germany
[4]Center for Neuroscience and Center for Mind and Brain, University of California, Davis, Davis, CA 95618, USA
[5]Laboratory for Biomedical Microtechnology, Department of Microsystems Engineering (IMTEK) and the Bernstein Center Freiburg, Albert-Ludwigs-Universität Freiburg, 79110 Freiburg, Germany
[6]Department of Neurocognition, University of Maastricht, 6229 ER Maastricht, Netherlands
[7]These authors contributed equally to this work
*Correspondence: c.a.bosmanvittini@uva.nl (C.A.B.), pascal.fries@esi-frankfurt.de (P.F.)
http://dx.doi.org/10.1016/j.neuron.2012.06.037

SUMMARY

A central motif in neuronal networks is convergence, linking several input neurons to one target neuron. In visual cortex, convergence renders target neurons responsive to complex stimuli. Yet, convergence typically sends multiple stimuli to a target, and the behaviorally relevant stimulus must be selected. We used two stimuli, activating separate electrocorticographic V1 sites, and both activating an electrocorticographic V4 site equally strongly. When one of those stimuli activated one V1 site, it gamma synchronized (60–80 Hz) to V4. When the two stimuli activated two V1 sites, primarily the relevant one gamma synchronized to V4. Frequency bands of gamma activities showed substantial overlap containing the band of interareal coherence. The relevant V1 site had its gamma peak frequency 2–3 Hz higher than the irrelevant V1 site and 4–6 Hz higher than V4. Gamma-mediated interareal influences were predominantly directed from V1 to V4. We propose that selective synchronization renders relevant input effective, thereby modulating effective connectivity.

INTRODUCTION

During natural vision, many stimuli simultaneously activate our visual system. In primary visual cortex, two separate stimuli typically activate two separate groups of neurons. These separate groups of neurons send anatomical connections that converge onto postsynaptic neurons in higher visual areas (Fries, 2009). Through this convergence, the postsynaptic neurons can respond to either one of the two stimuli. Yet, if one of those stimuli is behaviorally relevant, it dominates the activity of the postsynaptic neurons at the expense of the irrelevant stimulus (Moran and Desimone, 1985; Treue and Maunsell, 1996; Reynolds et al., 1999). This effect can be explained as a selective enhancement of synaptic gain of the relevant input (Reynolds et al., 1999). A candidate mechanism for this enhancement needs to fulfill at least the following criteria: (1) it has to be specific for the relevant subset of synaptic inputs versus the irrelevant subset, even though the two sets are probably interspersed on a postsynaptic neuron; (2) it has to be flexible to select different subsets of synapses as the relevant stimulus undergoes changes; and (3) it has to be able to switch within a few hundred milliseconds from strengthening one set of synapses to another set, because switching attention from one stimulus to another affects the activity of the postsynaptic neurons and behavior at this time scale (Busse et al., 2008).

To meet these requirements, we and others have proposed that the selective enhancement of relevant synaptic input is implemented by the selective rhythmic synchronization of the neuronal target group with the relevant input (Fries, 2005, 2009; Börgers and Kopell, 2008). Rhythmic activity in a target group entails corresponding fluctuations in postsynaptic membrane potentials and postsynaptic shunting, which render input most effective if it is consistently timed to the peaks of depolarization, i.e., if it is synchronized with the target. This hypothesis has been termed "Communication through Coherence," or CTC (Fries, 2005). It has been implemented in mathematical models that demonstrate its plausibility and the strength with which it can affect neuronal interactions (Börgers and Kopell, 2008; Tiesinga and Sejnowski, 2010; Buehlmann and Deco, 2010; Akam and Kullmann, 2010).

There is already experimental support for the mechanistic prediction of the CTC hypothesis: when two groups of neurons are rhythmically active, then the strength of their interaction depends on the phase relation between their rhythms (Womelsdorf et al., 2007). When three rhythmically active groups are considered, one of them can at the same time be in phase and therefore interacting with a second group, while being out of

phase and therefore noninteracting with a third group. We aim here to test the cognitive prediction of the CTC hypothesis, i.e., that a neuronal target group synchronizes selectively with those input neurons that provide behaviorally relevant input.

CTC is consistent, yet goes beyond a previous proposal that considered the synchronization only among the input neurons and stated that enhanced synchronization among behaviorally relevant input neurons increases their impact onto postsynaptic target neurons through feedforward coincidence detection. Tests of this previous proposal obviously confined themselves to assessing the synchronization within the input neuron group. These studies revealed that neurons activated by an attended as compared to an unattended stimulus show enhanced gamma-band synchronization in monkey area V4 (Fries et al., 2001, 2008; Taylor et al., 2005; Bichot et al., 2005; Buffalo et al., 2011) and area V2 (Buffalo et al., 2011) and either reduced (Chalk et al., 2010), unchanged, or enhanced (Buffalo et al., 2011) gamma-band synchronization in area V1. For area V4, the enhancements of gamma-band synchronization have been shown to be functionally relevant: a key behavioral consequence of attention, an enhanced speed of change detection, is predicted selectively by neuronal synchronization in the gamma-frequency range, but not by synchronization in other frequency ranges or by neuronal firing rates (Womelsdorf et al., 2006; Hoogenboom et al., 2010).

While enhanced gamma-band synchronization among relevant input neurons is fully consistent with the CTC hypothesis, CTC crucially entails that those neurons achieve an exclusive or selective synchronization to their postsynaptic target neurons at the expense of competing, behaviorally irrelevant input neurons. Through this, CTC lends a central mechanistic role to the rhythm of the neuronal target group: it is the synchronization of this rhythm to the rhythm of the relevant stimulus input that enhances the gain of this input. Testing this central prediction requires the simultaneous activation of two competing inputs and the simultaneous recording of the rhythm in the group of neurons providing input and the rhythm in their target group. To enable a concrete experimental test of CTC, a strong prediction can be derived about the synchronization among local rhythms in monkey areas V1 and V4 during selective attention to one of two simultaneously presented visual stimuli: if two stimuli activate separate sites in V1, and both activate one V4 site equally strongly, then the V4 site should synchronize selectively to the V1 site driven by the attended stimulus. Here, we test this prediction, assessing local rhythms through electrocorticographic (ECoG) local field potential (LFP) recordings.

RESULTS

To quantify synchronization between V1 and V4, we used multisite LFP recordings, which have been shown highly effective in assessing long-range, interareal synchronization (Roelfsema et al., 1997; von Stein et al., 2000; Tallon-Baudry et al., 2001, 2004). Multisite LFP recordings are routinely carried out with ECoG grid electrodes implanted onto the brains of epilepsy patients for presurgical focus localization. These unique recordings from the human brain have been used for numerous cognitive and/or systems neuroscience studies (Tallon-Baudry et al., 2001; Canolty et al., 2006), yet they typically do not include early visual areas. We therefore developed a high-density ECoG grid of electrodes (1 mm diameter platinum discs) and implanted it subdurally onto the brains of two macaque monkeys to obtain simultaneous recordings from 252 electrodes across large parts of the left hemisphere (Rubehn et al., 2009).

Figure 1A shows the brain of monkey P with the electrode positions superimposed (see Figure S1A, which shows electrode positions for both monkeys, available online). Figure 1B illustrates that a contralateral visual stimulus induced strong gamma-band activity (Gray et al., 1989), while an ipsilateral stimulus did not. Figure S1B shows respective time-frequency analyses, demonstrating that stimulus-induced gamma was sustained as long as the stimulus was presented. The gamma band was within the range of frequencies described in previous studies using drifting gratings in human subjects or awake monkeys (Hoogenboom et al., 2006; Fries et al., 2008; Muthukumaraswamy et al., 2009; Swettenham et al., 2009; Vinck et al., 2010; van Pelt et al., 2012). Within that range, the gamma band found here was relatively high, most likely due to the individual predispositions of the animals and the use of moving stimuli (Swettenham et al., 2009) of high contrast (Ray and Maunsell, 2010). Figure 1C shows for several V1 example electrodes (green dots in Figure 1A) receptive fields (RFs) in the form of enhanced gamma-band power in response to visual stimulation in specific parts of the lower right visual field quadrant (see Experimental Procedures and Figure S1C for details). The well-defined RFs indicate that a given electrode was primarily assessing neuronal activity in a small patch of the underlying visual cortex. Figure 1D shows respective examples for several V4 electrodes (red dots in Figure 1A). In both V1 and V4, the ordered representation of eccentricity and elevation was as predicted by numerous previous studies (Gattass et al., 2005). Figure S1D shows RF outlines from two recording sessions separated by 2 months, illustrating the stability of RF positions and thereby suggesting that the electrodes were in a stable position on the cortex.

With these recordings at hand, we engaged the monkeys in the selective visual attention task illustrated in Figure 1E (see Experimental Procedures for details). When the monkey touched a bar and fixated a central dot, two patches of drifting grating appeared. The two stimuli were always blue and yellow, with the color assigned randomly. After about 1 s, the fixation point assumed the color of one of the stimuli, which was thereby cued as relevant. In each trial, the relevant grating changed curvature at an unpredictable moment up to 4.5 s after the cue, and the monkey was rewarded for bar releases within a short time window thereafter. Changes in the irrelevant grating were equally probable, but corresponding bar releases were not rewarded. In monkeys K and P, 92% and 94% of bar releases, respectively, were correct reports of changes in the relevant stimulus. In 10% of the trials, only one or the other stimulus was shown in isolation (and its changes had to be reported) to assess stimulus selectivity of the recording sites.

For all analyses, we used the period from 0.3 s after cue onset until one of the stimuli changed. Also, for all further analyses, we first calculated local bipolar derivatives, i.e., differences between LFPs from immediately neighboring electrodes. We refer to the bipolar derivatives as "sites." Bipolar derivation further

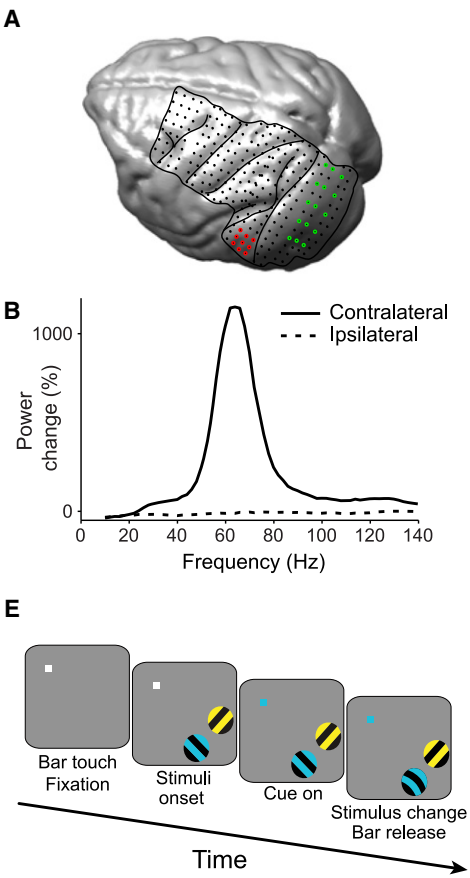

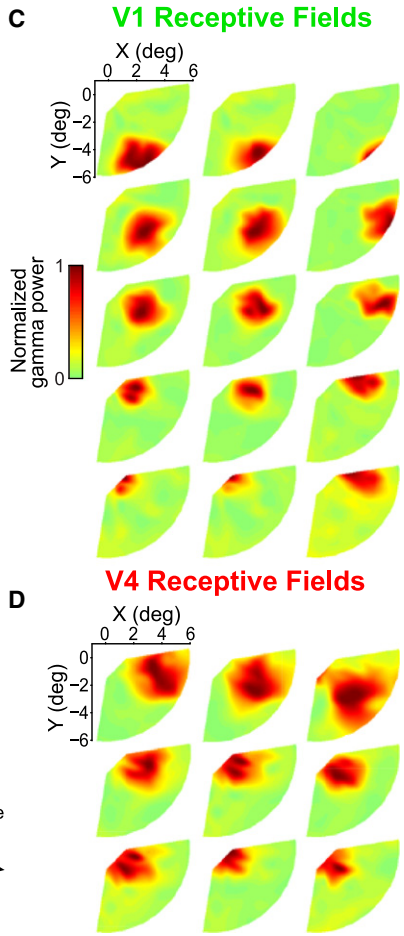

Figure 1. High-Density Monkey ECoG Grid and Attention Paradigm

(A) Rendering of the brain of monkey P. Lines indicate the covered area with the major sulci. Dots indicate the 252 subdural electrodes.

(B) Power change relative to baseline in a V1 electrode for contra- and ipsilateral stimulation.

(C) Receptive fields of the 3 × 5 V1 example electrodes shown in green in (A).

(D) Receptive fields of the 3 × 3 V4 example electrodes shown in red in (A). Color bar applies to (C) and (D).

(E) Selective attention paradigm. See Experimental Procedures for details. See also Figure S1.

enhances spatial specificity of the signal and removes the common recording reference, which is important for the analysis of synchronization between sites.

Figure 2 shows the results for a single data set including a V4 site activated equally by each of two stimuli and two V1 sites activated exclusively by either one or the other stimulus. Figures 2A–2F illustrate the stimulus selectivity of the different sites during isolated stimulation with stimulus 1 (condition marked red in Figure 2A) or stimulus 2 (condition marked blue in Figure 2A); site "V4" was equally driven by both stimuli (Figure 2B); site "V1a" responded to stimulus 1, but not 2 (Figure 2C); the opposite was the case for site "V1b" (Figure 2D). Figures S2A–S2D show the respective raw power spectra. Figures 2E and 2F demonstrate that V4 showed pronounced interareal synchronization in the 60–80 Hz band selectively with the V1 site that was stimulus driven. In the following, we will refer to the 60–80 Hz band as the gamma band. Figure S1E shows the topography across V1 and V4 of stimulus-induced gamma-band power changes and of the gamma-band coherence relative to the V4 site. Coherence showed a peak in V1 that coincided with the V1 power-change peak.

Figure 2G illustrates the selective attention conditions with both stimuli presented simultaneously but only one stimulus behaviorally relevant and therefore selected in any given trial. In the V4 site, attention to either stimulus gave essentially the same activation (Figure 2H), confirming that the site was equally driven by either stimulus. In both V1 sites, attention to their respective driving stimulus led to a slight but highly consistent increase in the frequency of the gamma-band activity (Figures 2I and 2J; $p < 0.001$ for both V1a and V1b, nonparametric randomization test on peak frequency). This shift was clearly visible also in the raw power spectra (Figures S2G and S2H). Crucially, Figures 2K and 2L demonstrate that the V4 site gamma band synchronized almost exclusively to the attended V1 site ($p < 0.001$ for both V1a and V1b, nonparametric randomization test on gamma-band coherence, see Experimental Procedures for details), despite the fact that both V1 sites were driven equally strongly.

The presence of coherence between two sites implies neither zero-phase relationship nor symmetry of mutual influence. To investigate the mutual influences between the example V1 and V4 sites, we determined Granger-causal (GC) influences in the bottom-up and the top-down directions. The GC influence of time series A onto time series B quantifies the variance in B that is not explained by the past of B but by the past of A (Kamiński et al., 2001; Dhamala et al., 2008). Figures 3B–3E show GC-influence spectra during isolated stimulation with either stimulus 1 (red condition) or stimulus 2 (blue condition). V4 was bottom-up GC influenced in the gamma band selectively by the V1 site that was stimulus driven (Figures 3B and 3C; $p < 0.001$ for both V1a and V1b, nonparametric randomization test). Similarly, V4 exerted a top-down GC influence in the gamma band selectively to the V1 site that was stimulus driven (Figures 3D and 3E; $p < 0.05$ for both V1a and V1b, same test). Figures 3G–3J show GC-influence spectra when both stimuli were presented simultaneously, but only stimulus 1 (red condition) or stimulus 2 (blue condition) were behaviorally relevant. V4 was bottom-up GC influenced in the gamma band almost exclusively by the relevant V1 site (Figures 3G and 3H; $p < 0.001$ for both V1a and V1b, same test). Similarly, V4 exerted

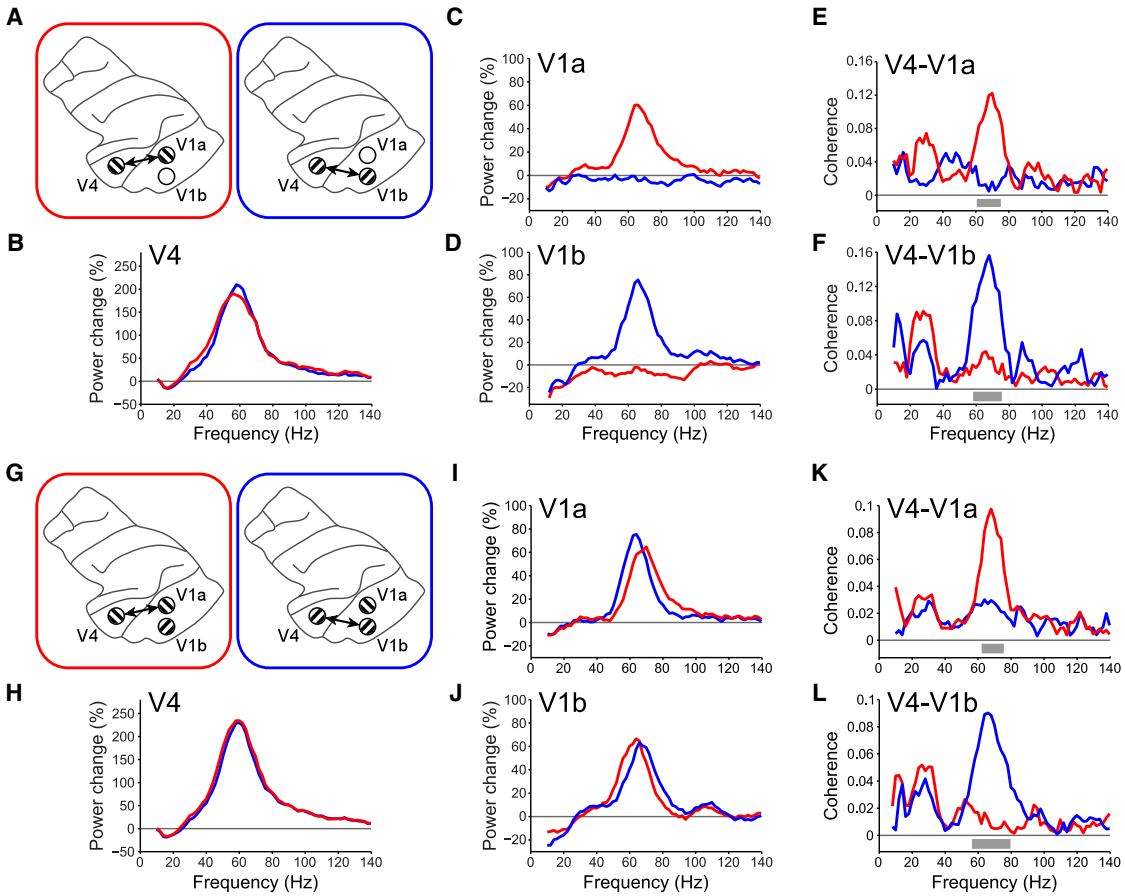

Figure 2. Example Triplet Recording of One V4 and Two V1 Sites in Monkey P

(A) Illustration of the two single-stimulus conditions. The red and blue boxes color code the two single-stimulus conditions for (B)–(F). Both conditions activated V4 but only the condition labeled red (blue) activated site V1a (V1b). The double arrow illustrates the likely pattern of interaction between neuronal groups.

(B–D) Spectral power changes (relative to prestimulus baseline) for the sites in V4 (B), V1a (C), and V1b (D).

(E and F) Coherence spectra for the site pairs V4-V1a (E) and V4-V1b (F). Gray bars indicate frequencies with a significant effect ($p < 0.05$, corrected for multiple comparisons across frequencies, nonparametric randomization across epochs). (B)–(F) use 249 epochs of 0.5 s per condition.

(G) Illustration of the two attention conditions with simultaneous presentation of both stimuli and attentional selection of one or the other stimulus. The red and blue boxes color code the two attention conditions for (H)–(L). The arrows indicate the selective interaction of the V4 site with the behaviorally relevant V1 site.

(H–J) Spectral power changes (relative to prestimulus baseline) for the sites in V4 (H), V1a (I), and V1b (J).

(K and L) Coherence spectra for the site pairs V4-V1a (K) and V4-V1b (L). Gray bars represent same test as in (E) and (F). (H)–(L) use 1,102 epochs of 0.5 s per condition. See also Figure S2 for absolute power spectra.

a top-down GC influence in the gamma band primarily to the relevant V1 site (Figures 3I and 3J; $p < 0.05$, same test). Please note that gray bars below the spectra result from frequency-wise tests followed by multiple comparison correction, while this text reports tests applied directly to the gamma band (see Experimental Procedures for details). Because the latter approach does not require multiple comparison correction and integrates the frequency bins of the gamma band before testing, it is more sensitive.

These effects of selective attention on power, and on interareal coherence and GC influences, were consistent across our sample of paired V1-V4 recordings (Figures 4, 5, and 6), although not always as pronounced as in the example. In V1, we selected sites that were primarily driven by one of the two stimuli. By contrast, in V4, we selected sites that were driven similarly by both stimuli (see Experimental Procedures for details). Correspondingly, for V4, condition assignment was arbitrary and Figure 4A shows V4 power changes (relative to prestimulus baseline) averaged across attention conditions, illustrating robust stimulus-induced gamma-band activation. Figure 4B shows the same analysis for V1 sites, split for attention inside and outside the V1-RF. Attention raised the V1 gamma peak frequency ($p < 0.001$, nonparametric test based on randomization across sites; $n = 37$ sites) but did not change V1 gamma peak amplitude (not significant [n.s.], same test). Figure 4C shows the coherence spectra averaged across all V1-V4 pairs of both monkeys, split by whether attention was inside or outside the V1-RF. Selective attention enhanced gamma-band coherence by 76% ($p < 0.001$, nonparametric randomization test across site pairs; $n = 88$ pairs of sites). The data from Figure 4C

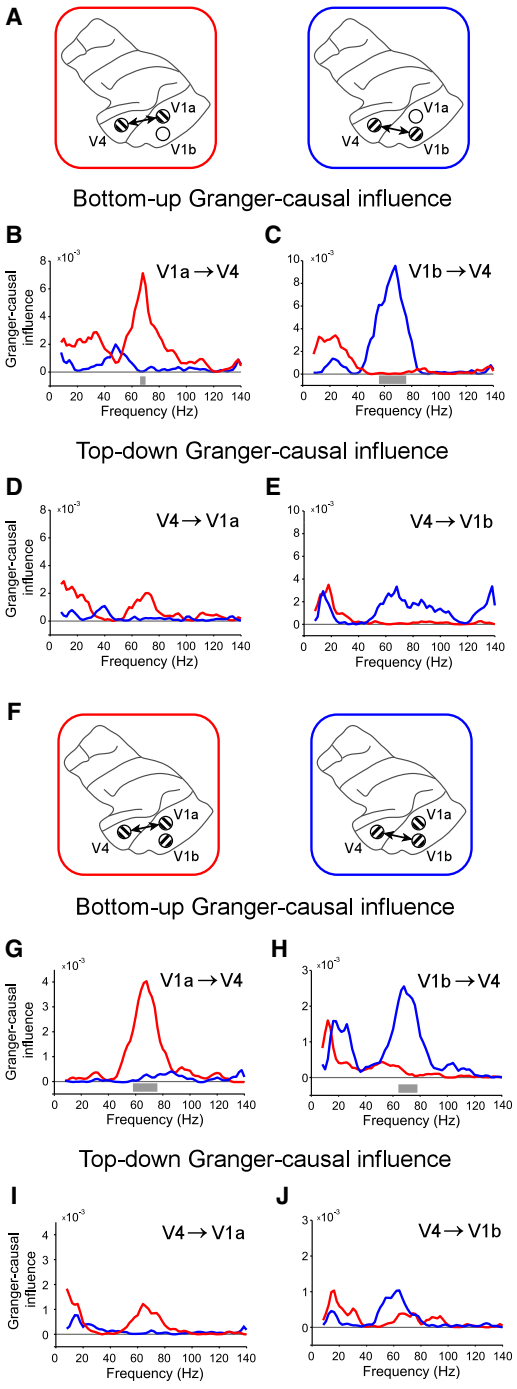

Figure 3. Analysis of GC Influences for the Same Example Triplet as Shown in Figure 2

(A) Illustration of the two single-stimulus conditions. The red and blue boxes color code the two single-stimulus conditions for (B)–(E).

(B–E) Frequency-wise GC influences from V1a to V4 (B), from V1b to V4 (C), from V4 to V1a (D), and from V4 to V1b (E).

(F) Illustration of the two attention conditions with simultaneous presentation of both stimuli and attentional selection of one or the other stimulus. The red and blue boxes color code the two attention conditions for (G)–(J).

(G–J) Frequency-wise GC influences from V1a to V4 (G), from V1b to V4 (H), from V4 to V1a (I), and from V4 to V1b (J). Gray bars indicate frequencies with a significant effect ($p < 0.05$, corrected for multiple comparisons across frequencies, nonparametric randomization across epochs). (B)–(E) use 249 epochs of 0.5 s per condition. (G)–(J) use 1,102 epochs of 0.5 s per condition.

are shown separately per monkey in Figures 4D and 4E; in monkey P, attention enhanced gamma-band coherence by 56% ($p < 0.001$, same test; $n = 68$), and this average contained several very clear examples as, e.g., the one shown in Figure 2. In monkey K, attention enhanced gamma-band coherence by 142% ($p < 0.001$, same test; $n = 20$). Figure 4F shows the underlying distributions of gamma-band coherence values for each V1-V4 pair and session in the two attention conditions ($p < 0.001$ based on a paired sign test; $n = 400$).

Figure 5 shows the gamma peaks of the two individual monkeys, scaled to ease comparison of peak frequencies. Between the two individuals, the gamma-frequency bands are distinctly different, as has been reported previously for animals (Vinck et al., 2010) and humans (Hoogenboom et al., 2006; Muthukumaraswamy et al., 2009; Swettenham et al., 2009; van Pelt et al., 2012). Within the individual gamma-frequency bands, both monkeys showed the same arrangement of gamma peak frequencies: the gamma peak frequency at the relevant V1 site was 2–3 Hz higher than at the irrelevant V1 site and 4–6 Hz higher than at the V4 site. Importantly, the differences in gamma peak frequencies should not be taken as evidence that the respective gamma rhythms were not coupled, because we found clear V1-V4 coherence. The presence of coherence demonstrates that phase relations are consistent across time. By contrast, uncoupled oscillators of different frequency would constantly precess relative to each other, leading to no consistent phase relation and an absence of coherence. We discuss possible reasons for the observed differences in power spectral peaks in the Discussion section.

Figures 6A and 6B show the average GC-influence spectra between V1 and V4, separately for the bottom-up (Figure 6A) and top-down (Figure 6B) directions, comparing attention inside the V1-RF (red lines) versus outside (blue lines). In the gamma band, selective attention enhanced the GC influence in the bottom-up direction by 134% ($p < 0.001$; $n = 88$) and in the top-down direction by 103% ($p < 0.001$; $n = 88$). In monkey P, in the gamma band, attention enhanced the GC influence in the bottom-up direction by 80% ($p < 0.001$; $n = 68$, Figure 6C), while there was no effect in the top-down direction (Figure 6D). In monkey K, in the gamma band, attention enhanced the GC influence in the bottom-up direction by 502% ($p < 0.001$; $n = 20$, Figure 6E) and in the top-down direction by 382% ($p < 0.001$; $n = 20$, Figure 6F).

The spectra of Figures 6A–6F are shown again in Figures 6G–6L, now separately for the conditions attention inside the V1-RF (Figures 6G, 6I, and 6K) and attention outside the V1-RF (Figures 6H, 6J, and 6L) and now comparing directly GC influences in the bottom-up direction (thick lines) versus top-down direction (thin lines). In the gamma band, with attention inside the V1-RF (Figure 6G), the GC influence in the bottom-up direction was 232% stronger than in the top-down direction ($p < 0.001$; $n = 88$). With attention outside, it was 100% stronger

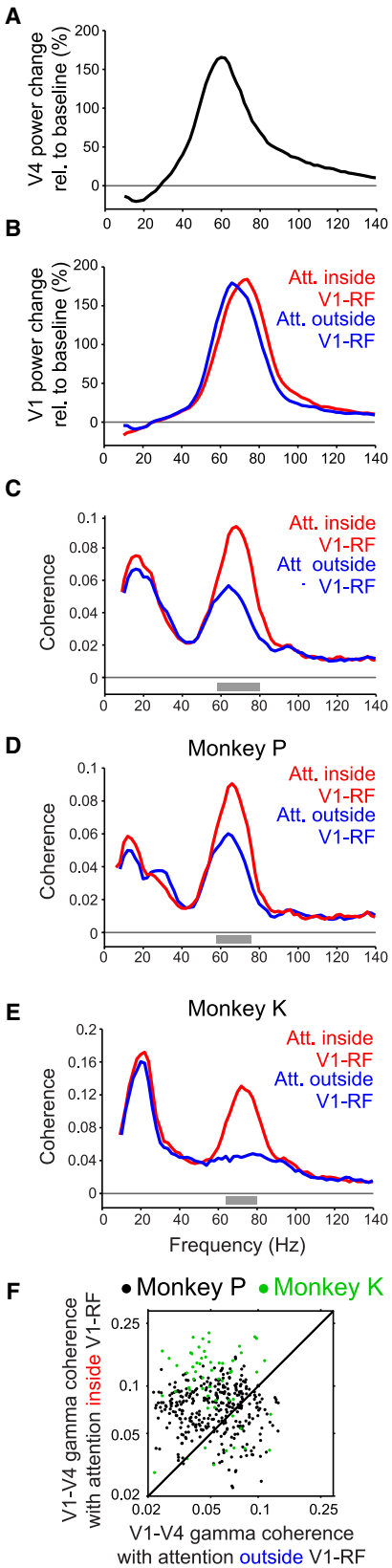

Figure 4. Average Results from the Attention Paradigm

(A) Average spectral power change relative to prestimulus baseline in V4.

(B) Average spectral power change relative to prestimulus baseline in V1, when the stimulus activating the respective site was behaviorally relevant (red) or irrelevant (blue).

(C) Average V1-V4 coherence spectrum, when the stimulus activating the respective V1 site was relevant (red) or irrelevant (blue). Gray bar indicates frequencies with a significant effect ($p < 0.05$, corrected for multiple comparisons across frequencies, nonparametric randomization across site pairs).

(D and E) The same analysis as (C) is shown but separately for monkey P (D) and monkey K (E).

(F) Scatter plot with each dot corresponding to a V1-V4 site pair and a recording session, comparing attention outside the V1-RF (x axis) to attention inside the V1-RF (y axis).

($p < 0.002$; $n = 88$, Figure 6H). In monkey P, the bottom-up compared to top-down influence was 298% stronger with attention inside the V1-RF ($p < 0.001$; $n = 68$, Figure 6I) and 101% with attention outside ($p < 0.002$; $n = 68$, Figure 6J). In monkey K, the bottom-up influence was 146% stronger with attention inside ($p < 0.005$; $n = 22$, Figure 6K), while there was no effect with attention outside (Figure 6L).

The mutual GC influences between time series A and B can artifactually appear higher in the A-to-B direction than vice versa if the signal-to-noise ratio (SNR) is higher for A than for B (Nalatore et al., 2007). To ensure that the differences between bottom-up and top-down GC influences are not due to differences in SNR, we stratified SNRs across the two areas. To ensure that attention effects on GC influences are not due to changes in SNR with attention, we stratified SNR across the two attention conditions. The details of the stratification are described in the Experimental Procedures section. The results of the stratified GC-influence analysis are shown in Figure S3 and confirm the nonstratified results.

Our finding that V4 is more gamma synchronized with the attended as compared to the unattended V1 group could be due to enhanced synchronization for the attended V1 group, reduced synchronization for the nonattended V1 group, or a combination of both effects. We were able to address this question, because the two stimuli were presented for at least 0.8 s before the fixation point changed color and cued one stimulus as relevant. Figure 7 shows the coherence spectra with attention inside or outside the V1 receptive fields as red and blue lines, respectively, and adds pink lines for the coherence spectra before the cue presentation. Precue coherence was similar to coherence with the V1 group activated by the irrelevant stimulus. Thus, the main effect of attention is to increase the coherence of V4 to the attended V1 group.

We performed a separate low-frequency analysis with reduced spectral smoothing for the typically narrower low-frequency bands (see Experimental Procedures for details). This analysis revealed no effect of attention that was consistent across both monkeys, neither for power nor for coherence.

A physiological theta rhythm (3–6 Hz) has been described in previous studies of area V4 (Lee et al., 2005; Fries et al., 2008; Bosman et al., 2009) and the theta phase has been found in many different brain areas to modulate the strength of local gamma-band activity (Bragin et al., 1995; Canolty et al., 2006; Bosman et al., 2009; Colgin et al., 2009; Fries, 2009). We

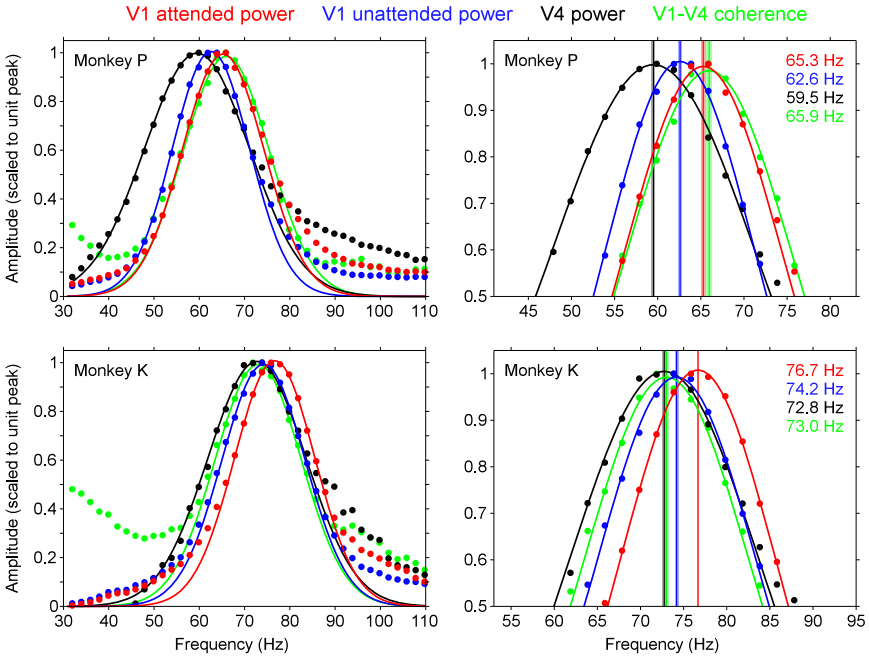

Figure 5. The Gamma Peaks of the Two Monkeys

All panels show the individual gamma peaks of the indicated monkeys. Area (combinations) and attention conditions are color coded as indicated at the top. The values of visually induced power and of coherence were divided by their respective maximum values in order to scale all peaks to unit peak height and thereby ease direct comparison of peak frequencies. Scaled spectra are shown as dots. Gaussians were fitted to the top third of each peak and are shown as solid lines (all R-square values were above 0.98). The panels on the right show the peaks in detail. The Gaussians' means, i.e., the gamma-band peaks, are shown as vertical lines (shaded regions correspond to 95% confidence bounds) and as numbers. See also Figure S5.

therefore investigated whether the long-range V1-V4 gamma-band coherence was modulated relative to peaks in the theta rhythm in V4. Figure 8A shows a respective time-frequency analysis from monkey K, suggesting a pronounced modulation of V1-V4 coherence in a 70–80 Hz band. Figure 8B shows that the 70–80 Hz V1-V4 coherence was modulated by 33% (peak-trough/mean; $p < 0.001$). Figure S4 shows the same analysis for monkey P, demonstrating that 60–70 Hz coherence was modulated by 21% ($p < 0.05$).

DISCUSSION

In summary, we have shown that V4 sites, which can synchronize with different V1 sites, do synchronize selectively with those V1 sites that are activated by the behaviorally relevant stimulus. To show this, we capitalized on multisite LFP recordings, because LFPs reflect local neuronal ensemble activities, and ensemble recordings enable a sensitive investigation of long-range interareal communication (Zeitler et al., 2006). The ensemble entrains its constituent single neurons (Fries et al., 2001; Womelsdorf et al., 2006) and, thereby, the observed interareal LFP coherence probably translates into interareal coherence among neuronal spiking.

Interareal gamma-band coherence has been shown through intracranial recordings in several previous publications (Engel et al., 1991a, 1991b; von Stein et al., 2000; Fell et al., 2001; Buschman and Miller, 2007; Womelsdorf et al., 2007; Gregoriou et al., 2009; Colgin et al., 2009; Popescu et al., 2009; Sigurdsson et al., 2010). For example, von Stein et al. investigated LFPs recorded from visual and associative brain areas of the awake cat and found correlations between gamma-filtered LFPs primarily for novel stimuli (von Stein et al., 2000). Similarly, Buschman and Miller investigated coherence between LFPs recorded in monkey frontal cortex and area LIP and found enhanced gamma-band coherence during bottom-up processing (Buschman and Miller, 2007). Gregoriou et al. investigated spike and LFP recordings from monkey areas V4 and FEF during the same selective attention task as used here. Pairs of V4 and FEF sites with overlapping RFs showed gamma-band coherence that was enhanced when attention was inside the joint RF (Gregoriou et al., 2009). Long-range gamma-band coherence has also been studied with noninvasive recordings in human subjects (Schoffelen et al., 2005, 2011; Siegel et al., 2008; Hipp et al., 2011). For example, Schoffelen et al. showed that corticospinal gamma-band coherence indexes a subject's dynamic movement preparation (Schoffelen et al., 2005) selectively among those corticospinal neurons involved in the upcoming movement (Schoffelen et al., 2011).

To study interareal coherence between monkey areas V1 and V4, we have relied on electrocorticographic LFP recordings that measure the electrical activity under the electrode. Neither the volume of tissue nor the way in which it affects the recording are fully understood. Yet, a few statements about ECoG recordings can be made. (1) ECoG signals do not provide a direct measure of spiking activity, and, therefore, our results do not directly test predictions that might be derived from the CTC hypothesis about spike synchronization. (2) ECoG recordings from V1 reflect both V1 neurons with connections to V4 and other V1 neurons. Similarly, ECoG recordings from V4 reflect V4 neurons with direct input from V1 and other V4 neurons. Therefore, our results do not directly quantify the coherence between V1 output neurons and their postsynaptic target neurons in V4. Such an analysis would have required the simultaneous recording of interareal pairs of isolated single units, identified to be monosynaptically coupled to each other. While this would have been technically extremely challenging, it would at the same time have rendered the analysis of interareal coherence extremely insensitive. Isolated single neurons reflect with their sparse spiking only poorly the phase of the underlying rhythm. For two isolated single neurons in V1 and V4, coherence analysis would have been exceedingly insensitive (Zeitler et al., 2006).

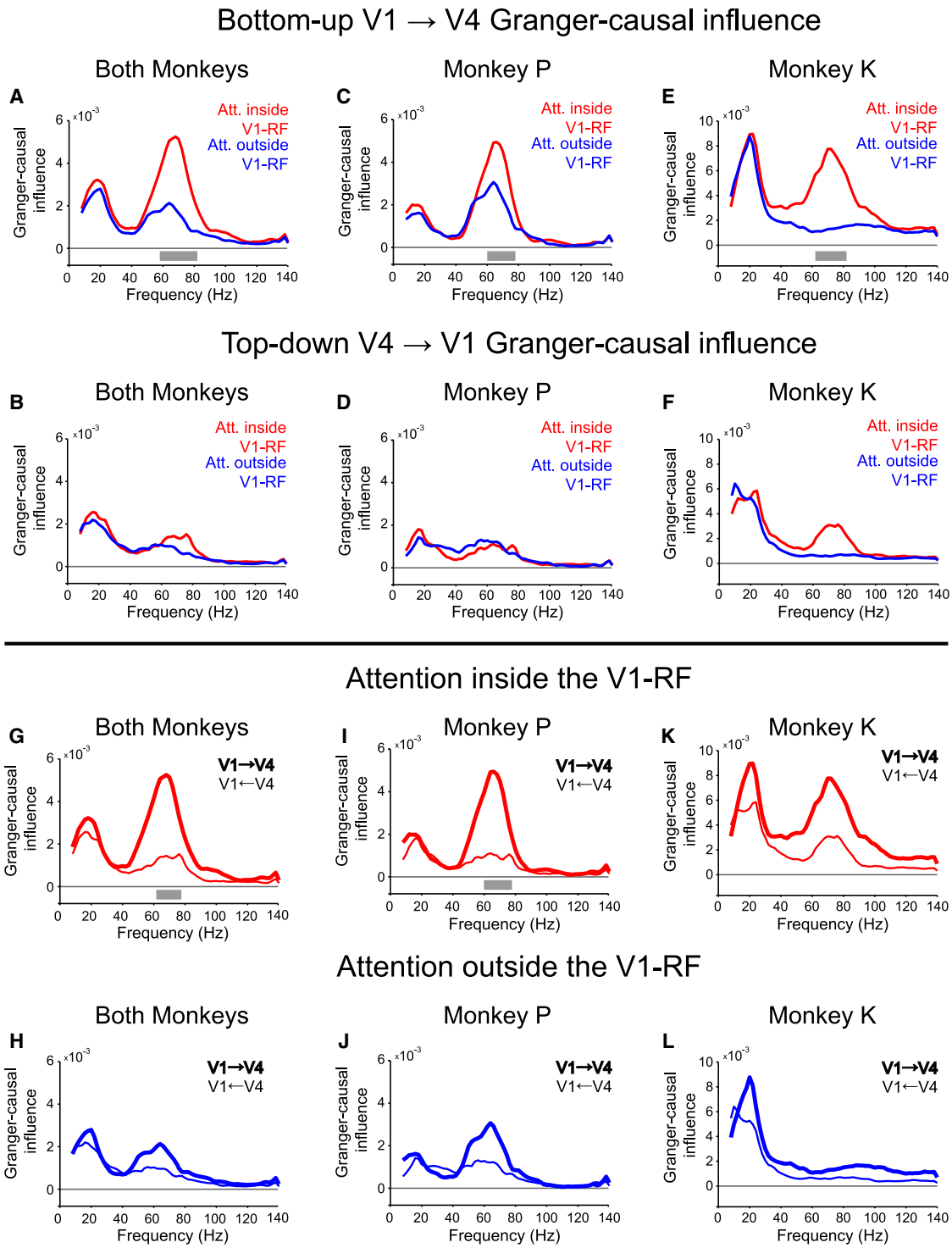

Figure 6. Average GC Influences

(A–F) Average GC-influence spectra between V1 and V4, separately for the bottom-up (A, C, and E) and top-down (B, D, and F) directions, comparing attention inside the V1-RF (red lines) versus outside the V1-RF (blue lines).

(A and B) Frequency-wise GC influences from V1 to V4 (A) and from V4 to V1 (B) for both monkeys combined.

(C and D) Frequency-wise GC influences from V1 to V4 (C) and from V4 to V1 (D) for monkey P.

(E and F) Frequency-wise GC influences from V1 to V4 (E) and from V4 to V1 (F) for monkey K.

(G–L) The spectra of (A)–(F) are shown again in (G)–(L), now separately for the conditions attention inside the V1-RF (G, I, and K) and attention outside the V1-RF (H, J, and L) and now comparing directly GC influences in the bottom-up direction (thick lines) versus top-down direction (thin lines).

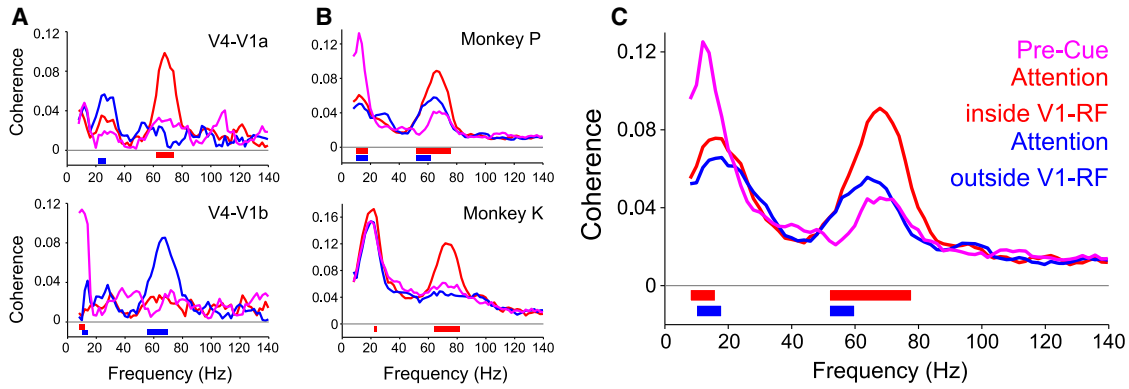

Figure 7. Coherence Spectra before and after Cue Presentation

(A) Coherence spectra between V4 and the indicated V1 site (same sites as Figure 2). The pink spectrum is from the precue epoch. The red (blue) spectrum is from the postcue epoch with attention inside (outside) the V1-RF. Colored bars indicate significant differences between the precue spectrum and the spectrum with the same color as the significance bar ($p < 0.05$, corrected for multiple comparisons across frequencies, nonparametric randomization across epochs).

(B) Same as (A) but giving the averages for the indicated monkeys and with statistics based on nonparametric randomization across site pairs.

(C) Same as (B) but giving the average across both monkeys. Please note that the postcue coherence spectra are not identical to those shown in Figures 2 and 4, because there were less precue than postcue epochs available and we therefore randomly subsampled postcue epochs to equate epoch numbers and avoid respective biases in the coherence estimate.

(3) ECoG recordings combine spatial resolution in the range of few millimeters (Figure 1C) with excellent sensitivity for the rhythms in the respective local neuronal population (Figure 1B). The core prediction of the CTC hypothesis with regard to selective attention relates to this mesoscopic level: the V4 rhythm is selectively coherent with the V1 rhythm that is driven by the behaviorally relevant stimulus. To test this prediction, simultaneous multiarea ECoG recordings are ideal.

Spike recordings in V4 would have allowed testing whether postsynaptic neurons responded primarily to the attended stimulus. However, this core result from the attention field (Moran and Desimone, 1985; Reynolds et al., 1999) has been replicated several times and presumably holds also in our experiment. Thereby, our present results actually also support the "Binding by Synchronization" (BBS) hypothesis. The BBS hypothesis states that distributed neurons, activated by the same stimulus, are bound together by synchronization (Gray et al., 1989). Most studies testing the BBS hypothesis investigated distributed neuronal activations within a given area (Singer and Gray, 1995). Yet, a stimulus activates neurons distributed across several brain areas and the BBS hypothesis is meant to apply also to such interareal neuronal assemblies. As V4 neurons with two stimuli in their RF dynamically represent the attended stimulus, the BBS hypothesis predicts that they should dynamically synchronize to those V1 neurons that represent the same, i.e., the attended, stimulus. This prediction is confirmed by our present results.

Attention affected the gamma rhythm in area V1: while there was no significant attention effect on gamma power, there was a very reliable increase in gamma frequency. The absence of an attentional effect on gamma power in V1 disagrees with one previous study using small static bar stimuli (Chalk et al., 2010) and agrees with another previous study that used very similar stimuli and task as our paradigm (Buffalo et al., 2011). The attentional increase in gamma peak frequency has not been reported before. It is intriguing, because attention to a stimulus is similar to an increase in stimulus contrast (Reynolds and Chelazzi, 2004), and higher contrast induces higher gamma-band frequencies in monkey area V1 (Figure S5A) (Ray and Maunsell, 2010). Higher contrast typically results in gamma power to increase (Henrie and Shapley, 2005; Chalk et al., 2010). Yet, for very high contrast levels, gamma power can saturate or even decrease, as is illustrated in Figure S5B, which explains why attention to our full-contrast stimuli did not lead to further gamma power enhancements.

Figure 5 shows that the local gamma peaks had a certain width, overlapping for their larger parts. While the gamma peak frequency at the relevant V1 site was 2–3 Hz higher than at the irrelevant V1 site, it was 4–6 Hz higher than in V4. If one considered these slightly different gamma peak frequencies without the coherence results, then the simplest interpretation would be the following: the rhythms at the attended V1 site, the unattended V1 site, and the V4 site reflect three independent sine wave oscillators with slightly, but distinctly different, frequencies; the width of the respective frequency bands is due to moment-to-moment deviations from perfect sine waves of the respective frequencies; those deviations are irrelevant noise. This interpretation entails that the three oscillators

(G and H) Frequency-wise GC influences with attention inside the V1-RF (G) and outside the V1-RF (H) for both monkeys combined.

(I and J) Frequency-wise GC influences with attention inside the V1-RF (I) and outside the V1-RF (J) for monkey P.

(K and L) Frequency-wise GC influences with attention inside the V1-RF (K) and outside the V1-RF (L) for monkey K. Gray bars indicate frequencies with a significant effect ($p < 0.05$, corrected for multiple comparisons across frequencies, nonparametric randomization across site pairs). See also Figure S3 for the same analysis after stratification for signal-to-noise ratios.

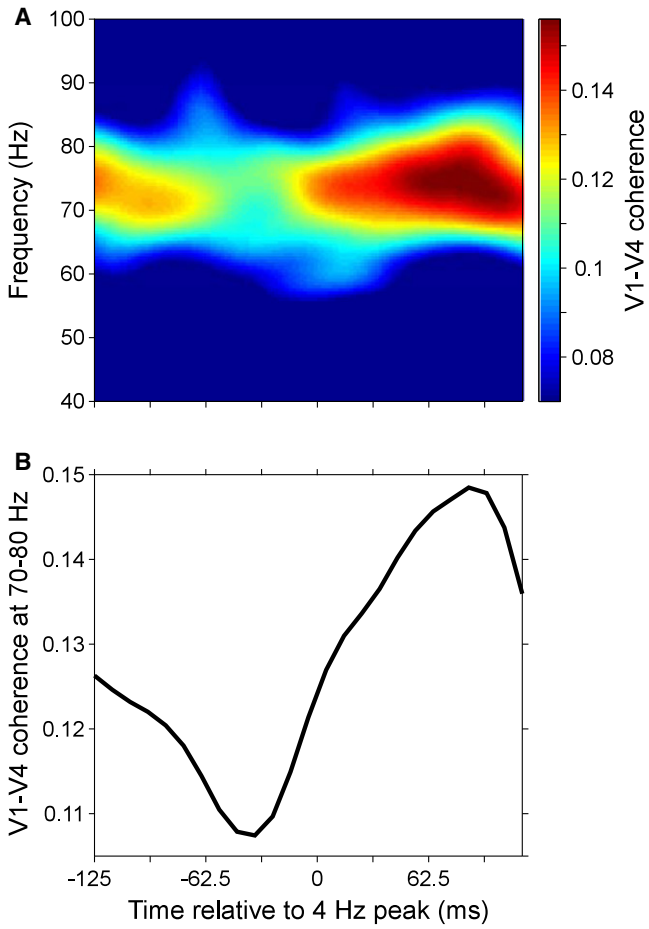

Figure 8. Cross-frequency Analysis of Interareal Synchronization as a Function of Time around the Theta Peak

(A) V1-V4 coherence as a function of time relative to peaks in the 4 Hz rhythm. (B) Coherence between V1 and V4 in a 70–80 Hz band, as a function of time relative to peaks in the 4 Hz rhythm. Data are from monkey K. See Figure S4 for data from monkey P.

constantly precess relative to each other, because their peak frequencies differ. For example, in monkey P, the V1-attended gamma peak frequency was 65.3 Hz and the V4 gamma peak frequency was 59.5 Hz (Figure 5), i.e., the peak frequencies differed by roughly 6 Hz. In the abovementioned interpretation, this would result in the relative gamma phase to precess over full 360° cycles roughly six times per second. Such a precession would result in fully inconsistent gamma phase relations and a complete absence of gamma coherence. Gamma coherence would actually be destroyed by any of the observed frequency differences: a 6 Hz frequency difference would lead to complete precession and loss of coherence six times per second, and a 2 Hz difference would lead to complete precession and loss of coherence two times per second. An absence of coherence would be inconsistent with CTC. However, we found clear V1-V4 gamma coherence. The presence of gamma coherence demonstrates that gamma phases did not freely precess against each other, but rather that gamma rhythms had a consistent phase relation. Thereby, the observation of coherence rules out the abovementioned simple interpretation of the slight frequency differences.

Rather, the synopsis of our findings suggests one of the following scenarios or a combination of them: (1) the frequencies of the synchronized rhythms at the V4 site and the relevant V1 site are always identical on a moment-by-moment basis, yet the common frequency fluctuates and the local circuits resonate at different frequencies, giving rise to different peak frequencies in the time-averaged power spectra; (2) our ECoG recordings in V4 reflect a mixture of (at least) two gamma rhythms in V4, one entrained by the attended V1 gamma and a second at a slightly lower frequency; and (3) in the third scenario, the different gamma frequencies play mechanistic roles in bringing about the selective interareal synchronization. There is one crucial additional ingredient to this scenario, namely a theta-rhythmic gamma-phase reset across V1 and V4, which we have described previously (Bosman et al., 2009). After the reset, the attended V1 gamma and the unattended V1 gamma partly precess relative to the slightly slower V4 gamma. The attended V1 gamma is of higher frequency than the unattended V1 gamma and therefore precesses faster. Correspondingly, in each gamma cycle, the attended V1 input enters V4 before the unattended V1 input. The earlier entry together with feedforward inhibition makes the attended V1 input entrain V4 at the expense of the unattended V1 input (Fries et al., 2007; Vinck et al., 2010). The selective entrainment of V4 by the attended V1 gamma rhythm further enhances the gain of the attended V1 input and reduces the gain of the unattended V1 input (Fries, 2005; Börgers and Kopell, 2008). The theta-rhythmic reset of interareal gamma-band synchronization is supported by our data (Figures 8 and S4). It probably corresponds to a reset of attentional selection and, under natural viewing conditions, might subserve the theta-rhythmic sampling of multiple objects in a scene, either overtly (Otero-Millan et al., 2008) or covertly (Fries, 2009; Landau and Fries, 2012).

Importantly, the third scenario, with partial precession, also leads to selective coherence, as observed here. The presence of coherence is not only necessary but also sufficient for CTC. CTC requires two rhythms with a phase relation that is (partly) consistent across time (or multiple observation epochs). The consistency of phase relations is precisely what is quantified by coherence. Crucially, coherence entails that the phase estimates of the two signals do not reflect noise, because with a pure noise signal on either one of the sides, phase relations would be random and there would be no coherence. Thereby, coherence in itself demonstrates (1) the presence of two meaningful rhythms on the two sides and (2) the presence of synchronization. As exemplified in the above scenarios, coherence does not require that two sites show rhythms with the same or similar peak frequency. And we note also that rhythms with the same or similar peak frequency are not sufficient for coherence. If, e.g., the two visual hemispheres are separated by cutting the corpus callosum, then the gamma rhythms in the two hemispheres of a given animal are essentially identical, but there is no coherence (Engel et al., 1991a).

We found that Granger-causal influences in the gamma band were substantially stronger in the bottom-up V1-to-V4 direction

than vice versa. Granger analyses alone can ultimately not prove or disprove one particular network organization. Yet, the strong bottom-up directedness of the V1-V4 gamma GC influence combines with two additional pieces of evidence: (1) both in V1 and V4, neuronal spiking is gamma synchronized almost exclusively in the superficial layers, while neuronal spiking in infragranular layers lacks gamma synchronization (Buffalo et al., 2011), and (2) V1 neurons projecting to V4 are located almost exclusively in supragranular layers, while V4 neurons projecting to V1 are located almost exclusively in infragranular layers (Barone et al., 2000). These three pieces of evidence together suggest that (1) in V1, gamma synchronization emerges in supragranular layers, and the behaviorally relevant V1 gamma influences V4 through feedforward projections with their respective delay; (2) in V4, gamma synchronization also emerges in supragranular layers and primarily influences areas further downstream of V4; and (3) the top-down influence from V4 to V1 originates from deep V4 layers and is therefore mediated to a much lesser extent through the gamma band. A direct test of these predictions will require laminar recordings in both areas simultaneously.

Most importantly, we demonstrate strong interareal gamma-band synchronization that links V4 dynamically to the relevant part of V1, precisely as predicted by the CTC hypothesis. The CTC hypothesis states that a local neuronal rhythm modulates input gain rhythmically, that input is therefore most effective if it is consistently timed to moments of maximal gain, and that thereby the synchronization between input and target modulates effective connectivity (Fries, 2005, 2009; Schoffelen et al., 2005, 2011; Womelsdorf et al., 2007; van Elswijk et al., 2010). The context-dependent modulation of effective connectivity is at the heart of cognition. A paradigmatic case for this is selective attention, in which relevant stimulus input is routed preferentially, and the result of this selective routing can be read directly from the activity of the target neurons (Moran and Desimone, 1985; Treue and Maunsell, 1996; Reynolds et al., 1999). Our current results strongly suggest that the selective routing of attended input is implemented by selective gamma-band synchronization between the target and the attended input, according to the CTC mechanism.

EXPERIMENTAL PROCEDURES

Visual Stimulation and Attention Paradigm

All procedures were approved by the ethics committee of the Radboud University, Nijmegen, NL. Stimuli and behavior were controlled by the software CORTEX (http://www.cortex.salk.edu). Stimuli were presented on a cathode ray tube (CRT) monitor at 120 Hz noninterlaced. When the monkey touched a bar, a gray fixation point appeared at the center of the screen. When the monkey brought its gaze into a fixation window around the fixation point (0.85° radius in monkey K; 1° radius in monkey P), a prestimulus baseline of 0.8 s started. If the monkey's gaze left the fixation window at any time, the trial was terminated. The measured eye positions during correct trials used for analysis differed only by an average of 0.03° of visual angle between the two attention conditions. After the baseline period, two physically isoluminant patches of drifting sinusoidal grating appeared (diameter: 1.2°; spatial frequency: 0.4–0.8 cycles/deg; drift velocity: 0.6 deg/s; resulting temporal frequency: 0.24–0.48 cycles/s; contrast: 100%). The two grating patches chosen for a given recording session always had equal eccentricity, size, contrast, spatial frequency, and drift velocity. The two gratings always had orientations that were orthogonal to each other, and they had drift directions that were incompatible with a Chevron pattern moving behind two apertures, to avoid preattentive binding. Positions and sizes of the two stimuli were aimed to achieve the following: (1) there should be one or more sites in area V4 that were activated by the two stimuli to an equal amount and (2) there should be one or more sites in area V1 that were activated by only one of the two stimuli.

In any given trial, one grating was tinted yellow, the other blue, with the color assigned randomly across trials. The yellow and blue colors were physically equiluminant. After 1–1.5 s (0.8–1.3 s in monkey P), the fixation point changed color to match the color of one of the two gratings, thereby indicating this grating as the relevant stimulus and the other as irrelevant. For each trial, two independent change times for the two stimuli were determined randomly between stimulus onset and 4.5 s after cue onset, according to a slowly rising hazard rate. If the relevant stimulus changed (before or after the irrelevant stimulus changed) and the monkey released the bar within 0.15–0.5 s thereafter, the trial was terminated and a reward was given. If the monkey released the bar at any other time, the trial was terminated without reward. The stimulus changes were small changes in the grating pattern, with the stripes undergoing a gentle bend (Figure 1E). During the bend, the outer ends of the grating stripes lagged increasingly behind the center of the stripes, until the lag reached 0.1° at 75 ms after the start of the bend. Over the course of another 75 ms, the stripes straightened again. We used this shape-change detection task, because previous studies on gamma-band activity in monkey area V4 had found larger attention effects for a shape-tracking task (Taylor et al., 2005) than a color-change detection task (Fries et al., 2001, 2008).

On 10% of the trials, only one of the two stimuli was presented, randomly at one or the other position and tinted yellow or blue. In these trials, the fixation point always assumed the color of this one grating, the change time was determined according to the same hazard rate, and if the monkey released within 0.15–0.5 s thereafter, a reward was given.

Several sessions (either separate or after attention-task sessions) were devoted to the mapping of receptive fields, using 60 patches of moving grating, as illustrated in Figure S1C. Receptive field positions were stable across recording sessions (Figure S1D).

Neurophysiological Recording Techniques and Signal Preprocessing

Neuronal recordings were made from two left hemispheres in two monkeys through a micromachined 252-channel electrocorticogram-electrode array implanted subdurally (Rubehn et al., 2009). Briefly, a 6.5 × 4 cm craniotomy over the left hemisphere in each monkey was performed under aseptic conditions with isoflurane anesthesia. The dura was opened and the ECoG was placed directly onto the brain under visual control. Several high-resolution photos were taken before and after placement of the ECoG for later coregistration of ECoG signals with brain regions. After ECoG implantation, both the bone and the dural flap were placed back and secured in place. After a recovery period of approximately 3 weeks, we started with neuronal recordings.

Signals obtained from the 252 electrode grid were amplified 20 times by eight Plexon headstage amplifiers, then low-pass filtered at 8 kHz and digitized at 32 kHz by a Neuralynx Digital Lynx system. LFP signals were obtained by low-pass filtering at 200 Hz and downsampling to 1 kHz. Powerline artifacts were removed by digital notch filtering. The actual spectral data analysis included spectral smoothing that rendered the original notch invisible.

Data Analysis General

All analyses were done in MATLAB (MathWorks) and using FieldTrip (Oostenveld et al., 2011) (http://fieldtrip.fcdonders.nl).

For the analysis of the data recorded during the attention task, we used the time period from 0.3 s after cue onset (the change in the fixation point color) until the first change in one of the stimuli. For each trial, this period was cut into nonoverlapping 0.5 s data epochs, discarding remaining time at the end of the period that was less than 0.5 s long.

We calculated local bipolar derivatives, i.e., differences (sample-by-sample in the time domain) between LFPs from immediately neighboring electrodes. We refer to the bipolar derivatives as "sites." Bipolar derivation further

enhances spatial specificity of the signal and removes the common recording reference, which is important when analyzing synchronization between sites. Subsequently, per site and individual epoch, the mean was subtracted, and then, per site and session, the signal was normalized by its standard deviation. These normalized signals were pooled across sessions with identical stimulus and task, unless indicated otherwise.

Spectral Analysis

Spectral power, coherence, and GC influences were estimated by applying a fast Fourier transform (FFT) after multitapering (Mitra and Pesaran, 1999) with seven tapers. Given epoch lengths of 0.5 s, this resulted in a spectral smoothing of ±7 Hz. The resulting spectra are shown from 8 Hz to 140 Hz. We performed a separate analysis of the lower frequencies (4 Hz to 28 Hz), in which the same 0.5 s data epochs were Hanning tapered. This did not reveal any consistent attentional effect.

For the analysis of GC influences, we applied nonparametric spectral matrix factorization to the cross-spectral density (Dhamala et al., 2008). We performed this factorization separately for each pair of sites. GC influence spectra were first estimated with the same spectral concentration parameters as all spectra and then smoothed with a two-frequency-bin boxcar window. If in a site pair one site has a higher SNR, then the analysis of GC influences has a bias toward estimating a stronger influence from the high-SNR site to the low-SNR site (Nalatore et al., 2007). To control for this, we stratified for SNR. We defined SNR as the absolute power of the bipolar-derived, -demeaned, and SD-normalized signal in the frequency band for which the stratification was intended. There were two types of comparisons related to the Granger analysis and two corresponding types of stratification. (1) We compared bottom-up with top-down GC influences. In this case, we stratified SNR per site pair across the two areas. (2) We compared GC influences in a given direction between two attention conditions. In this case, we stratified SNR per site pair across the two attention conditions.

In both cases, per site pair, trials were discarded until the mean SNR was essentially identical (and the SNR distribution across trials was as similar as possible) across sites (case 1) or across attention conditions (case 2). If for a given site pair this left fewer than 100 trials, the site pair was discarded from the stratified analysis.

Statistical Testing

Statistical testing included two steps: we first tested across all frequencies for significances at a $p < 0.05$ level, while correcting for multiple comparisons across frequencies. We found significant differences in bands that are indicated as gray bars in the spectra and that fell almost entirely into the frequency band of 60–80 Hz. We therefore averaged within this 60–80 Hz band to report effect sizes and corresponding precise significance levels in the text.

We assessed the significance of differences between conditions with a nonparametric randomization test. We first will explain the procedure for the example of Figure 2K, testing the significance of the difference in coherence between attention conditions. First, the coherence spectra were calculated across all epochs per condition. If more epochs were available for one condition, a random subset was chosen to equate epoch numbers and corresponding biases. The difference between the two coherence spectra is the observed coherence difference spectrum. Second, 1,000 randomizations were performed. In each randomization, the following steps were performed: (1) the epochs from both conditions were randomly redistributed into two sets of equal size; (2) the two randomized coherence spectra were determined; (3) the corresponding randomized coherence difference spectrum was determined; and (4) only the maximum and the minimum of this difference spectrum was retained and entered into two randomization distributions, for maximal and minimal differences.

For each frequency of the observed coherence difference spectrum, the difference was compared to the two randomization distributions. If the difference was smaller than the 2.5th percentile of the minimal randomization distribution or larger than the 97.5th percentile of the maximal randomization distribution, it was considered significant at a $p < 0.05$ level. This corresponds to a two-sided test with multiple comparison correction across frequencies. The multiple comparison correction results from the fact that for each randomization, only the maximal and minimal differences across all frequencies entered into the randomization distributions (Nichols and Holmes, 2002; Maris et al., 2007). Frequencies with significant coherence differences are marked with a gray bar in all figures.

This procedure, as explained for the example coherence spectrum, was applied similarly for the average across the entire sample of coherence spectra. The only difference was that, for each randomization, the random condition assignment was done per coherence spectrum contributing to the average, rather than per epoch. The same approach as used for coherence spectra was also applied to GC influence spectra.

Similar randomization procedures were also used for the average across the 60–80 Hz band and for gamma peak frequencies or amplitudes: the observed difference was compared to the randomization distribution of differences. A correction for multiple comparisons was not necessary in this case. Statistical testing for the cross-frequency interaction is described below.

Site Selection

The main requirement for V1-V4 site pairs to be included in the analysis was that the V4 site had to be driven roughly equally by the two stimuli, while the V1 site had to be driven primarily by one of the two stimuli. In order to employ an objective selection, sites and site pairs had to satisfy a number of quantitative criteria. The results that we report were robust against moderate changes in those criteria. Obviously, coherence and corresponding attention effects got weaker when, e.g., sites were included that were not properly stimulus driven or pairs of sites whose receptive fields did not overlap well. The selection was performed according to the following steps.

(1) For each site, we normalized power spectra to make the values more directly interpretable. We calculated the gamma-band power (P; 40–100 Hz) averaged across all prestimulus baseline periods (Pb) and during stimulation (Ps). We calculated normalized power spectra during stimulation (nPs): $nPs = (Ps - Pb) / Pb$.

(2) We selected those sites that were driven by the stimuli. In V1 and V4, we selected all sites for which nPs during simultaneous presentation of both stimuli, i.e., during the two conditions of the attention task pooled, was 0.2 or larger.

(3) For each site, we calculated a response map (RM), as shown in Figures 1C and 1D, using the data from the RF mapping (sub)sessions. We created a spatial map of nPs for the 60 different mapping stimuli (Figure S1C), smoothed this map with a Gaussian kernel, and normalized it to values between zero and one.

(4) From the driven sites (step 2), we selected sites with RFs that overlapped well with one of the stimuli used in the attention paradigm. To calculate the overlap, we multiplied the site's response map with the respective stimulus map, i.e., a map with the value one where the stimulus fell and zero everywhere else, and subsequently summed across space. We selected sites whose overlap with one of the stimuli exceeded 30% of the distribution across the driven sites.

(5) We selected V1-V4 site pairs that had some chance of being anatomically connected, based on a quantification of overlap between their response maps. We multiplied the V1-RM with the V4-RM and summed across space. We selected pairs whose overlap exceeded 30% of the distribution across the driven sites. RF overlap was positively related to V1-V4 gamma-band coherence (Figure S1F).

(6) In V1, we selected those sites that had a preference for one of the two stimuli. We calculated a stimulus selectivity index (SI) by relating the gamma-band power induced by the two stimuli, i.e., Ps1 and Ps2, respectively: $SI = (Ps1 - Ps2) / (Ps1 + Ps2)$. We selected those V1 sites for which the absolute value of the selectivity index was 0.4 or larger. This created one group (Gs1) of sites with preference for stimulus 1 and one group (Gs2) with preference for stimulus 2.

(7) In V4, we selected those sites that were roughly equally driven by the two stimuli. We calculated the same selectivity index as in V1 but selected sites with a selectivity index (absolute value) of 0.1 or smaller.

(8) We excluded those V1 sites that, despite their relative preference for one stimulus, still picked up activity induced by the other stimulus. To this end, we did the following. For each site in Gsx (x being 1 or 2), we calculated the coherence spectrum to all sites in Gsy (y being 2

if x was 1 and vice versa). We averaged all those coherence spectra. If they showed coherence, this was a sign that the Gsx site picked up activity induced by stimulus 2. Thus, we eliminated a Gsx site if its average coherence spectrum to all Gsy sites was not flat. In order to quantify whether a coherence spectrum was flat, we compared it to its bias estimate. We estimated the coherence bias by shuffling all trials before calculating coherence. Those bias estimates were subtracted for each Gsx-Gsy pair before averaging the coherence spectra between a given Gsx site and all Gsy sites. The average bias-subtracted coherence spectra were then rectified and summed across all frequencies. The resulting value had to be smaller than 0.06.

Cross-frequency Analysis

We analyzed the effect of the theta frequency phase in V4 on the high-frequency synchronization between V1 and V4 as follows. The phase of the V4 theta oscillation was determined from a set of average referenced sites overlying V4. Signals obtained from these sites were band-pass filtered between 3 and 5 Hz, and the time points of the peaks of the low-frequency oscillation were determined using the Hilbert transform, after averaging across sites. Subsequently, we computed the time-frequency representation of V1-V4 coherence, time locked to the peak of the low-frequency V4 theta oscillation. We only included those trials for a given V1-V4 pair when the stimulus encoded by the V1 site was the attended stimulus. Coherence was computed using a frequency-dependent sliding window of ten cycles, between 40 and 100 Hz, in steps of 2 Hz. The resulting time-frequency representations showed high coherence in the gamma band in slightly different bands for both monkeys (monkey K: 70–80 Hz, monkey P: 60–70 Hz). The magnitude of coherence seemed to systematically change as a function of the low-frequency phase. We evaluated this statistically by performing a nonparametric randomization test and repeated the following procedure 1,000 times. We randomly permuted the sequence of the individual peak-locked analysis windows. This shuffling essentially destroyed the temporal profile of the phase of the theta oscillation and served to construct a null distribution of the amplitude of a cosine function (with a frequency of 4 Hz) fitted to the temporal profile of V1-V4 coherence in a predefined frequency band. The estimated amplitude of the cosine function from the unshuffled data was tested against this distribution to obtain a p value.

SUPPLEMENTAL INFORMATION

Supplemental Information includes five figures and can be found with this article online at http://dx.doi.org/10.1016/j.neuron.2012.06.037.

ACKNOWLEDGMENTS

We thank Mark Roberts and Eric Lowet for support, Edward Chang for help with implanting monkey P, Mingzhou Ding for providing the code for spectral matrix factorization, and Karl Friston and Wolf Singer for helpful comments on earlier versions of this manuscript. This work was supported by the European Young Investigator program of the European Science Foundation (P.F.), the European Union's seventh framework program (P.F.), the National Science Foundation Graduate Student Fellowship Program (A.M.B.), and a Fulbright grant from the U.S. Department of State (A.M.B.). R.O. and J.-M.S. gratefully acknowledge the support of the BrainGain Smart Mix Programme of the Netherlands Ministry of Economic Affairs and the Netherlands Ministry of Education, Culture, and Science.

Accepted: June 22, 2012
Published: September 5, 2012

REFERENCES

Akam, T., and Kullmann, D.M. (2010). Oscillations and filtering networks support flexible routing of information. Neuron *67*, 308–320.

Barone, P., Batardiere, A., Knoblauch, K., and Kennedy, H. (2000). Laminar distribution of neurons in extrastriate areas projecting to visual areas V1 and V4 correlates with the hierarchical rank and indicates the operation of a distance rule. J. Neurosci. *20*, 3263–3281.

Bichot, N.P., Rossi, A.F., and Desimone, R. (2005). Parallel and serial neural mechanisms for visual search in macaque area V4. Science *308*, 529–534.

Börgers, C., and Kopell, N.J. (2008). Gamma oscillations and stimulus selection. Neural Comput. *20*, 383–414.

Bosman, C.A., Womelsdorf, T., Desimone, R., and Fries, P. (2009). A microsaccadic rhythm modulates gamma-band synchronization and behavior. J. Neurosci. *29*, 9471–9480.

Bragin, A., Jandó, G., Nádasdy, Z., Hetke, J., Wise, K., and Buzsáki, G. (1995). Gamma (40-100 Hz) oscillation in the hippocampus of the behaving rat. J. Neurosci. *15*, 47–60.

Buehlmann, A., and Deco, G. (2010). Optimal information transfer in the cortex through synchronization. PLoS Comput. Biol. *6*, e1000934.

Buffalo, E.A., Fries, P., Landman, R., Buschman, T.J., and Desimone, R. (2011). Laminar differences in gamma and alpha coherence in the ventral stream. Proc. Natl. Acad. Sci. USA *108*, 11262–11267.

Buschman, T.J., and Miller, E.K. (2007). Top-down versus bottom-up control of attention in the prefrontal and posterior parietal cortices. Science *315*, 1860–1862.

Busse, L., Katzner, S., and Treue, S. (2008). Temporal dynamics of neuronal modulation during exogenous and endogenous shifts of visual attention in macaque area MT. Proc. Natl. Acad. Sci. USA *105*, 16380–16385.

Canolty, R.T., Edwards, E., Dalal, S.S., Soltani, M., Nagarajan, S.S., Kirsch, H.E., Berger, M.S., Barbaro, N.M., and Knight, R.T. (2006). High gamma power is phase-locked to theta oscillations in human neocortex. Science *313*, 1626–1628.

Chalk, M., Herrero, J.L., Gieselmann, M.A., Delicato, L.S., Gotthardt, S., and Thiele, A. (2010). Attention reduces stimulus-driven gamma frequency oscillations and spike field coherence in V1. Neuron *66*, 114–125.

Colgin, L.L., Denninger, T., Fyhn, M., Hafting, T., Bonnevie, T., Jensen, O., Moser, M.B., and Moser, E.I. (2009). Frequency of gamma oscillations routes flow of information in the hippocampus. Nature *462*, 353–357.

Dhamala, M., Rangarajan, G., and Ding, M. (2008). Analyzing information flow in brain networks with nonparametric Granger causality. Neuroimage *41*, 354–362.

Engel, A.K., König, P., Kreiter, A.K., and Singer, W. (1991a). Interhemispheric synchronization of oscillatory neuronal responses in cat visual cortex. Science *252*, 1177–1179.

Engel, A.K., Kreiter, A.K., König, P., and Singer, W. (1991b). Synchronization of oscillatory neuronal responses between striate and extrastriate visual cortical areas of the cat. Proc. Natl. Acad. Sci. USA *88*, 6048–6052.

Fell, J., Klaver, P., Lehnertz, K., Grunwald, T., Schaller, C., Elger, C.E., and Fernández, G. (2001). Human memory formation is accompanied by rhinal-hippocampal coupling and decoupling. Nat. Neurosci. *4*, 1259–1264.

Fries, P. (2005). A mechanism for cognitive dynamics: neuronal communication through neuronal coherence. Trends Cogn. Sci. *9*, 474–480.

Fries, P. (2009). Neuronal gamma-band synchronization as a fundamental process in cortical computation. Annu. Rev. Neurosci. *32*, 209–224.

Fries, P., Reynolds, J.H., Rorie, A.E., and Desimone, R. (2001). Modulation of oscillatory neuronal synchronization by selective visual attention. Science *291*, 1560–1563.

Fries, P., Nikolić, D., and Singer, W. (2007). The gamma cycle. Trends Neurosci. *30*, 309–316.

Fries, P., Womelsdorf, T., Oostenveld, R., and Desimone, R. (2008). The effects of visual stimulation and selective visual attention on rhythmic neuronal synchronization in macaque area V4. J. Neurosci. *28*, 4823–4835.

Gattass, R., Nascimento-Silva, S., Soares, J.G., Lima, B., Jansen, A.K., Diogo, A.C., Farias, M.F., Botelho, M.M., Mariani, O.S., Azzi, J., and Fiorani, M. (2005). Cortical visual areas in monkeys: location, topography, connections, columns, plasticity and cortical dynamics. Philos. Trans. R. Soc. Lond. B Biol. Sci. *360*, 709–731.

Gray, C.M., König, P., Engel, A.K., and Singer, W. (1989). Oscillatory responses in cat visual cortex exhibit inter-columnar synchronization which reflects global stimulus properties. Nature *338*, 334–337.

Gregoriou, G.G., Gotts, S.J., Zhou, H., and Desimone, R. (2009). High-frequency, long-range coupling between prefrontal and visual cortex during attention. Science *324*, 1207–1210.

Henrie, J.A., and Shapley, R. (2005). LFP power spectra in V1 cortex: the graded effect of stimulus contrast. J. Neurophysiol. *94*, 479–490.

Hipp, J.F., Engel, A.K., and Siegel, M. (2011). Oscillatory synchronization in large-scale cortical networks predicts perception. Neuron *69*, 387–396.

Hoogenboom, N., Schoffelen, J.M., Oostenveld, R., Parkes, L.M., and Fries, P. (2006). Localizing human visual gamma-band activity in frequency, time and space. Neuroimage *29*, 764–773.

Hoogenboom, N., Schoffelen, J.M., Oostenveld, R., and Fries, P. (2010). Visually induced gamma-band activity predicts speed of change detection in humans. Neuroimage *51*, 1162–1167.

Kamiński, M., Ding, M., Truccolo, W.A., and Bressler, S.L. (2001). Evaluating causal relations in neural systems: granger causality, directed transfer function and statistical assessment of significance. Biol. Cybern. *85*, 145–157.

Landau, A.N., and Fries, P. (2012). Attention samples stimuli rhythmically. Curr. Biol. *22*, 1000–1004.

Lee, H., Simpson, G.V., Logothetis, N.K., and Rainer, G. (2005). Phase locking of single neuron activity to theta oscillations during working memory in monkey extrastriate visual cortex. Neuron *45*, 147–156.

Maris, E., Schoffelen, J.M., and Fries, P. (2007). Nonparametric statistical testing of coherence differences. J. Neurosci. Methods *163*, 161–175.

Mitra, P.P., and Pesaran, B. (1999). Analysis of dynamic brain imaging data. Biophys. J. *76*, 691–708.

Moran, J., and Desimone, R. (1985). Selective attention gates visual processing in the extrastriate cortex. Science *229*, 782–784.

Muthukumaraswamy, S.D., Edden, R.A., Jones, D.K., Swettenham, J.B., and Singh, K.D. (2009). Resting GABA concentration predicts peak gamma frequency and fMRI amplitude in response to visual stimulation in humans. Proc. Natl. Acad. Sci. USA *106*, 8356–8361.

Nalatore, H., Ding, M., and Rangarajan, G. (2007). Mitigating the effects of measurement noise on Granger causality. Phys. Rev. E Stat. Nonlin. Soft Matter Phys. *75*, 031123.

Nichols, T.E., and Holmes, A.P. (2002). Nonparametric permutation tests for functional neuroimaging: a primer with examples. Hum. Brain Mapp. *15*, 1–25.

Oostenveld, R., Fries, P., Maris, E., and Schoffelen, J.M. (2011). FieldTrip: Open source software for advanced analysis of MEG, EEG, and invasive electrophysiological data. Comput. Intell. Neurosci. *2011*, 156869.

Otero-Millan, J., Troncoso, X.G., Macknik, S.L., Serrano-Pedraza, I., and Martinez-Conde, S. (2008). Saccades and microsaccades during visual fixation, exploration, and search: foundations for a common saccadic generator. J. Vis. *8*, 21–1–18.

Popescu, A.T., Popa, D., and Paré, D. (2009). Coherent gamma oscillations couple the amygdala and striatum during learning. Nat. Neurosci. *12*, 801–807.

Ray, S., and Maunsell, J.H. (2010). Differences in gamma frequencies across visual cortex restrict their possible use in computation. Neuron *67*, 885–896.

Reynolds, J.H., and Chelazzi, L. (2004). Attentional modulation of visual processing. Annu. Rev. Neurosci. *27*, 611–647.

Reynolds, J.H., Chelazzi, L., and Desimone, R. (1999). Competitive mechanisms subserve attention in macaque areas V2 and V4. J. Neurosci. *19*, 1736–1753.

Roelfsema, P.R., Engel, A.K., König, P., and Singer, W. (1997). Visuomotor integration is associated with zero time-lag synchronization among cortical areas. Nature *385*, 157–161.

Rubehn, B., Bosman, C., Oostenveld, R., Fries, P., and Stieglitz, T. (2009). A MEMS-based flexible multichannel ECoG-electrode array. J. Neural Eng. *6*, 036003.

Schoffelen, J.M., Oostenveld, R., and Fries, P. (2005). Neuronal coherence as a mechanism of effective corticospinal interaction. Science *308*, 111–113.

Schoffelen, J.M., Poort, J., Oostenveld, R., and Fries, P. (2011). Selective movement preparation is subserved by selective increases in corticomuscular gamma-band coherence. J. Neurosci. *31*, 6750–6758.

Siegel, M., Donner, T.H., Oostenveld, R., Fries, P., and Engel, A.K. (2008). Neuronal synchronization along the dorsal visual pathway reflects the focus of spatial attention. Neuron *60*, 709–719.

Sigurdsson, T., Stark, K.L., Karayiorgou, M., Gogos, J.A., and Gordon, J.A. (2010). Impaired hippocampal-prefrontal synchrony in a genetic mouse model of schizophrenia. Nature *464*, 763–767.

Singer, W., and Gray, C.M. (1995). Visual feature integration and the temporal correlation hypothesis. Annu. Rev. Neurosci. *18*, 555–586.

Swettenham, J.B., Muthukumaraswamy, S.D., and Singh, K.D. (2009). Spectral properties of induced and evoked gamma oscillations in human early visual cortex to moving and stationary stimuli. J. Neurophysiol. *102*, 1241–1253.

Tallon-Baudry, C., Bertrand, O., and Fischer, C. (2001). Oscillatory synchrony between human extrastriate areas during visual short-term memory maintenance. J. Neurosci. *21*, RC177.

Tallon-Baudry, C., Mandon, S., Freiwald, W.A., and Kreiter, A.K. (2004). Oscillatory synchrony in the monkey temporal lobe correlates with performance in a visual short-term memory task. Cereb. Cortex *14*, 713–720.

Taylor, K., Mandon, S., Freiwald, W.A., and Kreiter, A.K. (2005). Coherent oscillatory activity in monkey area v4 predicts successful allocation of attention. Cereb. Cortex *15*, 1424–1437.

Tiesinga, P.H., and Sejnowski, T.J. (2010). Mechanisms for phase shifting in cortical networks and their role in communication through coherence. Front. Hum. Neurosci. *4*, 196.

Treue, S., and Maunsell, J.H. (1996). Attentional modulation of visual motion processing in cortical areas MT and MST. Nature *382*, 539–541.

van Elswijk, G., Maij, F., Schoffelen, J.M., Overeem, S., Stegeman, D.F., and Fries, P. (2010). Corticospinal beta-band synchronization entails rhythmic gain modulation. J. Neurosci. *30*, 4481–4488.

van Pelt, S., Boomsma, D.I., and Fries, P. (2012). Magnetoencephalography in twins reveals a strong genetic determination of the peak frequency of visually induced γ-band synchronization. J. Neurosci. *32*, 3388–3392.

Vinck, M., Lima, B., Womelsdorf, T., Oostenveld, R., Singer, W., Neuenschwander, S., and Fries, P. (2010). Gamma-phase shifting in awake monkey visual cortex. J. Neurosci. *30*, 1250–1257.

von Stein, A., Chiang, C., and König, P. (2000). Top-down processing mediated by interareal synchronization. Proc. Natl. Acad. Sci. USA *97*, 14748–14753.

Womelsdorf, T., Fries, P., Mitra, P.P., and Desimone, R. (2006). Gamma-band synchronization in visual cortex predicts speed of change detection. Nature *439*, 733–736.

Womelsdorf, T., Schoffelen, J.M., Oostenveld, R., Singer, W., Desimone, R., Engel, A.K., and Fries, P. (2007). Modulation of neuronal interactions through neuronal synchronization. Science *316*, 1609–1612.

Zeitler, M., Fries, P., and Gielen, S. (2006). Assessing neuronal coherence with single-unit, multi-unit, and local field potentials. Neural Comput. *18*, 2256–2281.